# Subthreshold oscillations and resonant frequency in guinea-pig cortical neurons: physiology and modelling

Yoram Gutfreund, Yosef Yarom and Idan Segev

*Department of Neurobiology and Center for Neuronal Computation, Institute of Life Sciences, Hebrew University, Jerusalem 91904, Israel*

1. Intracellular recordings were made from neurons in slices from guinea-pig frontal cortex. In 50% of the cells, sustained subthreshold voltage oscillations were evoked by long (>6 s) depolarizing pulses. The peak-to-peak amplitude of these oscillations was less than 5 mV and the frequency was voltage dependent, increasing with depolarization from 4 (near rest) to 20 Hz (at 30 mV depolarization).

2. The impedance–frequency relationship of both oscillating and non-oscillating cells was studied by intracellular injection of sinusoidal current with linearly changing frequency. In most cells, a peak in the impedance magnitude (resonant behaviour) was observed at depolarized levels. The frequency of the peak impedance (peak frequency) increased with depolarization from 3 (near rest) to 15 Hz (at 30 mV depolarization).

3. Application of TTX ($10^{-6}$ M) significantly decreased the impedance magnitude near the peak frequency. The subthreshold oscillations, however, as well as the action potentials, were fully blocked by TTX. On the other hand, TEA (15 mM) and $Cs^+$ (5 mM) abolished both the subthreshold oscillations and the resonant behaviour. Replacing $Ca^{2+}$ with $Co^{2+}$ (5 mM) or $Ni^{2+}$ (1 mM) did not abolish the subthreshold oscillations. The peak in the frequency–response curve was only slightly reduced.

4. An isopotential membrane model, consisting of a leak current, a fast persistent sodium current, a slow non-inactivating potassium current (with the kinetics of the M-current) and membrane capacitance, is sufficient to produce both voltage oscillations and resonant behaviour. The kinetics of the $K^+$ current by itself is sufficient to produce resonance behaviour. The $Na^+$ current amplifies the peak impedance magnitude and is essential for the generation of subthreshold oscillation. The model correctly predicted the behaviour of the frequency response before and after TTX and TEA application, as well as the relation between the expected passive impedance and the experimental impedance.

5. We speculate that the tendency of the neurons to generate voltage signals at a certain frequency (as a result of the subthreshold oscillations) and to preferentially respond to inputs arriving at the same frequency (the resonance behaviour) promotes population activity at that preferred frequency.

The electrical activity in the mammalian neocortex follows rhythms that may either dictate, or reflect the functional state of the brain (Adrian & Matthews, 1934). In spite of the prevalence of cortical rhythms, little is known about their mechanisms. There is strong evidence that at least some of these rhythms are driven by thalamocortical circuits (Steriade, McCormick & Sejnowski, 1993). On the other hand, cortical rhythmic activity has been measured in cortical slices (Silva, Amitai & Connors, 1991) indicating that rhythmic activity can arise from cortical local circuits. Synchronized rhythmic activity can emerge from a network of neurons that individually are non-oscillating (Getting, 1989). Another possibility is that the network rhythm is driven by individual neurons which are intrinsically oscillating (Steriade, Jones & Llinás, 1989). One cellular mechanism that may underlie rhythmicity in neuron assemblies is subthreshold voltage oscillation (Llinás, Grace & Yarom, 1991; Alonso & Klink, 1993).

Subthreshold oscillations have been described in neurons from several nuclei and structures within the mammalian nervous system (Willcox, Gutnick & Christoph, 1988; Silva *et al.* 1991; Alonso & Klink, 1993; Lampl & Yarom, 1993). These studies showed that subthreshold oscillations in various systems differ in their frequency, regularity and ionic mechanism. The theta rhythm measured from hippocampal tissue (which ranges from 4 to 10 Hz) has

been attributed to $Na^+$-dependent subthreshold oscillatory activity in neurons of the entorhinal cortex (Alonso & Klink, 1993). Cerebellar rhythmic activity, on the other hand, has been attributed to $Ca^{2+}$-dependent subthreshold oscillations in neurons from the inferior olive nucleus (Llinás & Yarom, 1986). Recently, Llinás *et al.* (1991) identified two types of subthreshold oscillations in the frontal cortex, one with a narrow bandwidth (35–50 Hz) and one, which is the focus of the present study, with a broad bandwidth of oscillations (10–45 Hz). It was suggested that this activity is the cellular substrate for rhythmic synchronized activity recorded by Gray, Konig, Engel & Singer (1989) from cortical networks during processing of sensory information.

In modelling the subthreshold electrical activity of excitable membranes, it has long been known that this activity can be simulated by adding an inductive component ($L$) to the traditional passive resistance–capacitance (RC) membrane model (Mauro, Conti, Dodge & Schor, 1970; Koch, 1984). Mauro *et al.* (1970) have shown that this apparent inductive component arises from time- and voltage-dependent conductances as formulated in the Hodgkin & Huxley (1952) model. In the frequency domain, such an inductive component, together with the membrane capacitance and resistance, will establish resonance behaviour with a preferred frequency. That is the frequency of a sinusoidal current input which gives rise to a *maximal* subthreshold voltage response. In the squid giant axon, this frequency is voltage dependent and is approximately 100 Hz (Mauro *et al.* 1970).

Resonant behaviour has been demonstrated in a wide variety of nerve cells: in hair cells from the cochlea of some vertebrates (Crawford & Fettiplace, 1981; Correia, Christensen, Moore & Lang, 1989); in electroreceptors in fish (Meyer & Zakon, 1982); and in several types of neurons in the mammalian nervous system (Gimbarzevsky, Miura & Puil, 1984; Puil, Meiri & Yarom, 1993). Interestingly, all the studies which demonstrated resonant behaviour also reported subthreshold oscillations (damped or sustained) for the same cells. This finding is not surprising in the light of electrical circuit theory which shows that a resonant peak in the frequency domain implies damped oscillations in the time domain. Consequently, frequency domain analysis can be a powerful tool for exploring and characterizing the mechanisms of subthreshold oscillations in excitable cells.

In the present work we focus our attention, both experimentally and theoretically, on two subthreshold properties of cortical pyramidal cells from guinea-pig frontal cortex: (1) the tendency of the membrane potential to oscillate, and (2) the resonant behaviour. Part of this work has been presented in abstract form (Gutfreund, Yarom & Segev, 1992).

# METHODS

Coronal slices from guinea-pig frontal cortex (13–15 mm from the earline; see Luparello, 1967) were used in this study. Guinea-pigs (weighing 200–300 g) of either sex were anaesthetized by I.P. injection of sodium pentobarbitone (35–60 mg $kg^{-1}$; Nembutal). Following anaesthesia the animals were decapitated, the brain rapidly removed and placed in aerated (95% $O_2$–5% $CO_2$) ice-cooled physiological solution for about 5 min. Six slices (300–400 $\mu$m) were cut on a vibratome sectioning system (TPI), and incubated in physiological solution at room temperature (20–25 °C) for over 1 h.

The submerged slice technique for recording was used throughout the study. The normal physiological solution that was used during experiments, as well as in the preparation and incubation of the slices, contained (mM): NaCl, 124; KCl, 5; $KH_3PO_4$, 1·2; $MgSO_4$, 1·3; $CaCl_2$, 2·4; $NaHCO_3$, 26; glucose, 10 (pH 7·4), bubbled with 95% $O_2$–5% $CO_2$. In those experiments in which TEA (15 mM) or $Cs^+$ (5 mM) was used, an equivalent amount of NaCl was removed. $Co^{2+}$ and $Ni^{2+}$ solutions were used to block $Ca^{2+}$ currents. In $Ni^{2+}$ solution, $NiCl_2$ replaced $CaCl_2$ (1 mM for 2·4 mM, respectively). $Co^{2+}$ solution was composed of (mM): NaCl, 132; KCl, 5; $MgCl_2$, 2; $CoCl_2$, 5; $NaHCO_3$, 22; glucose, 10. TTX was applied directly to the experimental chamber, reaching a final concentration of about $10^{-6}$ M. The solution was maintained at a constant temperature of 34 °C and flowed at a rate of 2–4 ml $min^{-1}$.

For intracellular recording and stimulation we used a high-input resistance amplifier with glass microelectrodes filled with 3 M potassium acetate (50–90 MΩ). In some experiments the electrodes were filled with 2(triethylamino)-*N*-(2,6-dimethylphenyl)acetamide (QX-314; 70 mM) dissolved in 3 M potassium acetate. All recordings were obtained from the dorsal part of the grey matter in the cortex where the cells are densely packed. Neurons with a stable resting potential and an action potential larger than 70 mV were used for the analysis. The results were either saved on floppy disk (via a digital oscilloscope; Nicollet 4094C), or converted to digital data through an MB-NIO-16 board (National Instruments) and analysed with a Macintosh-based labVIEW system.

### Transient analysis

The peeling method (Rall, 1969) was applied to estimate the system time constant, $\tau_0$, and the first equalizing time constant, $\tau_1$. The transient voltage response, $V$, to a short hyperpolarizing current pulse (0·6 ms; −3 nA) was used for this purpose. The input resistance, $R_{in}$, was estimated from the following formula (Durand, Carlen, Gurevich, Ho & Kunov, 1983):

$$R_{in} = \sum_{0}^{\infty} \frac{C_i \tau_i}{Iw}, \quad (1)$$

where $I$ is the amplitude and $w$ is the width of the injected current, $\tau_i$ is the time constant peeled from the transient response and $C_i$ are the corresponding coefficients (see details in Rapp, Segev & Yarom, 1994). For this estimation we used only the first two components (i = 0, 1).

### Oscillation analysis

The rhythmic nature of the subthreshold oscillations and their dominant frequency was analysed by calculating the autocorrelogram of the oscillating membrane voltage. The oscillation frequency was determined from the intervals between

the peaks of a 1 s long voltage autocorrelogram (Fig. 2*A–D*, right-hand traces). To obtain a more accurate estimate we averaged the results from four different sections of the voltage response (1 s each).

### Impedance analysis

The impedance ($Z$) amplitude profile (ZAP) method (Puil, Gimbarzevsky & Miura, 1986) was used to estimate the impedance of the system at low frequencies (< 50 Hz). The ZAP input function is an AC with a constant amplitude and a linearly changing frequency (Fig. 1*A*, lower trace). We used a home-made waveform generator to produce the ZAP input function. The amplitude of the ZAP input function was adjusted to keep the perturbation of the membrane potential smaller than 10 mV peak to peak. In the example shown in Fig. 1*A* (lower trace) the ZAP frequency is changing continuously and linearly from 20 to 0 Hz. The voltage response to this input current is shown in the upper trace of Fig. 1*A*. The input current and the voltage response were digitized at a sampling rate of 1000 $s^{-1}$ and transformed into the frequency domain using a fast Fourier transform (FFT). Figure 1*B* shows the FFT magnitude of the voltage response (FFT($V$)) and the current input (FFT($I$)) shown in Fig. 1*A*. The impedance of the system ($Z$) is a complex number defined as:

$$Z = Z_{\text{real}} + Z_{\text{imaginary}} = \frac{\text{FFT}(V)}{\text{FFT}(I)}. \quad (2)$$

The impedance was displayed in two forms: the impedance magnitude (IM) against frequency (IM plot; Fig. 1*C*) and the phase shift against frequency (Phase plot; Fig. 1*D*). It should be noted that part of the noise in both curves is due to the discrete transform procedure and it increases at the boundaries (see Bracewell, 1986). In order to decrease the noise we either used a five-point averaging algorithm (continuous line in Fig. 1*C* and

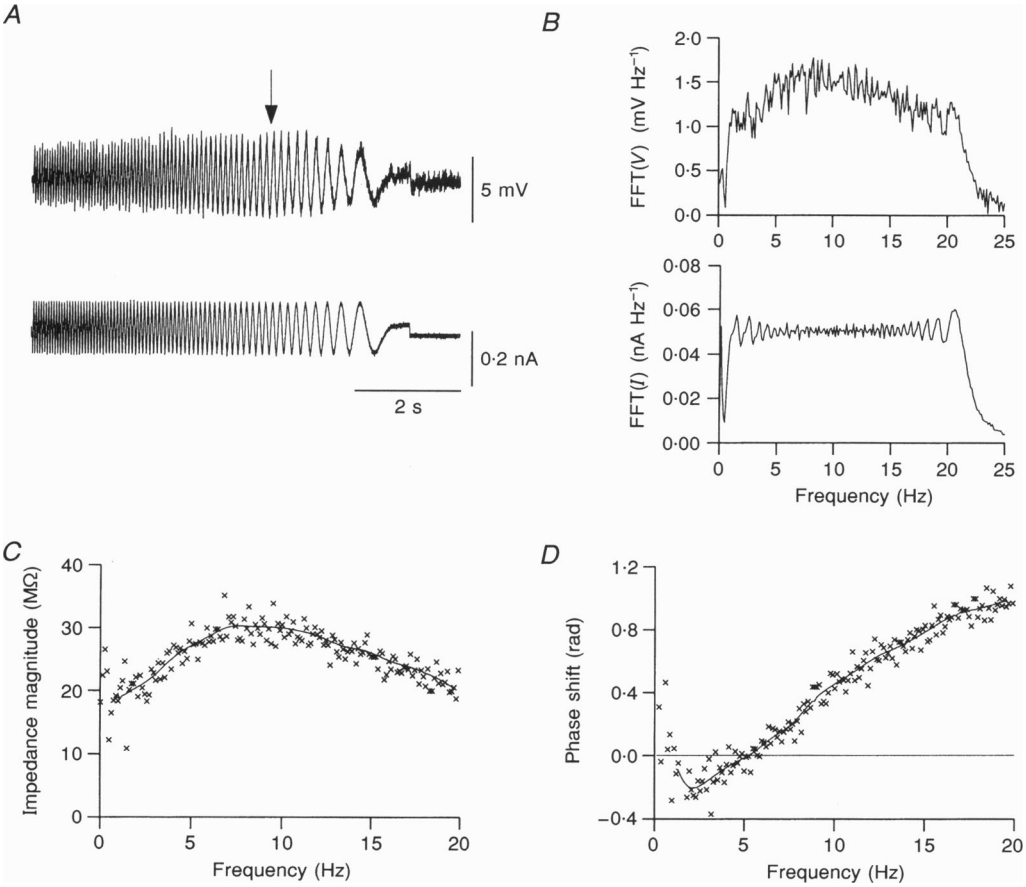


**Figure 1. The response of a cortical neuron to sinusoidal current with changing frequency (ZAP)**

*A*, voltage response (upper trace) to a ZAP current input (lower trace). The amplitude of the response depends on the input frequency, reaching a maximum approximately 5 s after stimulus onset (arrow). *B*, the FFT magnitude of the voltage response (FFT($V$), upper panel) and of the current input (FFT($I$), lower panel) of the signals shown in *A*. Note the peak in the FFT($V$) at about 10 Hz. *C*, the impedance magnitude as a function of frequency (IM plot) of the same cell. The continuous line represents the result of 50 × 5-point smoothing of the data. Because of the large error at the boundaries the data is smoothed from frequencies of 2 Hz and upwards. *D*, the phase shift between current input and voltage response. The continuous line represents the smoothed data. Note the phase advance (negative phase) at frequencies smaller than 5 Hz.

*D*) or averaged several sequential IM and phase plots (e.g. Fig. 4*F*). Because of the large error at the boundaries we ignored the data obtained in the first and last 2 Hz (e.g. in Fig. 1*C* and *D* the relevant range is 2–18 Hz).

In several control experiments we found that the electrode impedance was frequency independent in the range used in these experiments (0–50 Hz).

### Mathematical model

The modelled neuron was an isopotential RC compartment with three discrete transmembrane ionic currents flowing in parallel to the membrane capacitance (Fig. 11 in Appendix 1). Each of these currents was described using the Hodgkin & Huxley (1952) formalism (see Appendix 1). The current equation for this model is:

$$C\frac{dV}{dt} + I_{K,s} + I_{Na,p} + I_{leak} + I_{in} = 0, \quad (3)$$

where $C$, the membrane capacitance, was chosen to be 0·25 nF to fit a time constant of 10 ms with an input resistance of 40 MΩ which is close to the average values measured experimentally (see Results). $V$ is the membrane voltage; $t$ is time; $I_{K,s}$ is a slow non-inactivating potassium current which was described by the experimentally based equations for the M-current (a muscarinic potassium current) measured in the bullfrog sympathetic ganglion by Yamada, Koch & Adams (1989); $I_{Na,p}$ is a fast persistent non-inactivating sodium current. The formal description for this current was based on the analysis of hippocampal pyramidal neurons by French, Sah, Buckett & Gage (1990). Some of their original parameters were modified to fit our model (see Appendix 1). $I_{leak}$ is the passive leak current and $I_{in}$ is the ZAP input function given by:

$$I_{in} = A\sin(Bt^2) + DC, \quad (4)$$

where $A$, $B$ and $DC$ are constants designed to match the experimentally implemented stimulus function. In some of the simulations we added fast sodium spikes to the model. This was done by adding two additional voltage-dependent currents, a fast $Na^+$ current and a delayed $K^+$ current (Hodgkin & Huxley, 1952) to eqn (3). For a detailed description of the equations and parameters used in our model see Appendix 1.

### Numerical calculations

To explore the behaviour of the model in both frequency and time domains we used the numerical integration software Phaseplane (Ermentrout, 1990) with the Adam's integration option set on a step interval of 0·5 ms when simulating subthreshold oscillations or 0·05 ms when simulating both subthreshold oscillations and action potentials. The impedance functions were calculated using the same procedure as in the experimental part of the study.

### Analytical calculations

The impedance of the model about a specific steady state (SS) was calculated analytically by linearizing the current equation (eqn (3); e.g. Mauro *et al.* 1970; Koch, 1984; Hutcheon, Miura, Yarom & Puil, 1994). Briefly, the total current, $I$, is a function of membrane voltage ($V$) and membrane conductance ($g$). The differential of $I$ ($dI$), about the steady-state current input ($I_{ss}$), is given by:

$$\delta I = \left(\frac{\delta I}{\delta V}\right)_{ss}\delta V + \left(\frac{\delta I}{\delta V}\right)_{ss}\delta g. \quad (5)$$

Equation (5) is linear, therefore it is possible to evaluate directly the complex impedance ($Z$) about the SS which is defined as:

$$Z = \frac{\delta V}{\delta I}. \quad (6)$$

We note, however, that this approach gives only an approximation to the experimental situation where the perturbations are not infinitesimally small as assumed in the above linearization process. Still, as will be demonstrated below, the analytical solution was proven to be in agreement with the numerical results.

## RESULTS

### Subthreshold oscillations

We analysed the electrical behaviour of sixty-four cortical cells, most of which were probably pyramidal (intracellular injection of Lucifer Yellow revealed that eleven of twelve neurons tested were pyramidal). Based on electrophysiological criteria (McCormick, Connors, Lighthall & Prince, 1985), 17% of the cells were identified as intrinsic bursters (IBs) and the rest were regular spiking (RS) cells. Fast-spiking cells were not observed in this study. Table 1 summarizes several electrophysiological parameters of these cells.

The values in Table 1 are similar to those reported for cortical neurons in different areas of the neocortex (Connors, Gutnick & Prince, 1982; McCormick *et al.* 1985) except for the resting potential which was somewhat more depolarized than the values reported in these papers.

In eighteen of thirty-four cells subthreshold oscillatory activity could be elicited during an injection of a long depolarizing current pulse (> 6 s). An example of this behaviour is shown in Fig. 2. At resting level (Fig. 2*D*, left) a stable membrane potential was observed. Injection of 0·2 nA DC gave rise to 7 mV depolarization, on top of which low amplitude (1·52 ± 0·44 mV) oscillatory activity appeared (Fig. 2*C*, left). An increase in the DC to 0·3 nA depolarized the neuron to an average of 11 mV and elicited clear rhythmic oscillations with an amplitude of 3·7 ± 1·3 mV (Fig. 2*B*, left). Under these conditions, the larger amplitude of the oscillations was sufficient to occasionally reach threshold for spike firing. The action potentials were synchronized with the peak of the subthreshold oscillations (see also Llinás *et al.* 1991). A further increase in the frequency of the oscillations, accompanied by a decrease in amplitude, was observed when the DC was doubled to 0·6 nA (an average

**Table 1. Representative properties of recorded cells**

| Property | Mean ± S.D. | *n* |
|---|---|---|
| Input resistance (MΩ) | 36·7 ± 13·4 | 30 |
| Time constant (ms) | 11·2 ± 4·2 | 29 |
| Spike height (mV) | 87·9 ± 10·11 | 34 |
| Spike duration (ms)* | 1·38 ± 0·42 | 34 |
| Resting potential (mV) | −66 ± 9·2 | 10 |

* Measured at half-amplitude of action potential.

depolarization of 14 mV, Fig. 2*A*, left). The corresponding autocorrelograms of the voltage response (Fig. 2*A–D*, right-hand traces) demonstrate the rhythmic nature of these oscillations and the increase in frequency with depolarization. At 0·2 nA the frequency was 6 Hz (Fig. 2*C*, right), whereas at 0·6 nA it reached 11 Hz (Fig. 2*A*, right).

The frequency dependence of the subthreshold oscillations on the DC input was analysed in seven oscillating cells; an example is shown in Fig. 2*E*. This cell demonstrated a highly significant correlation between the frequency of subthreshold oscillations and the level of the injected DC ($P = 0{\cdot}0001$; one-way ANOVA). Six of the seven cells showed similar significant correlation ($P < 0{\cdot}05$). The average slope of the linear regression between the oscillation frequency and the DC was $14{\cdot}22 \pm 7{\cdot}4$ Hz nA$^{-1}$ ($n = 7$). The frequencies ranged from 4 Hz low amplitude currents (< 0·4 nA) to a maximum of 27 Hz at DC levels >1 nA. However, in only two cells did the maximum frequency exceed 17 Hz.

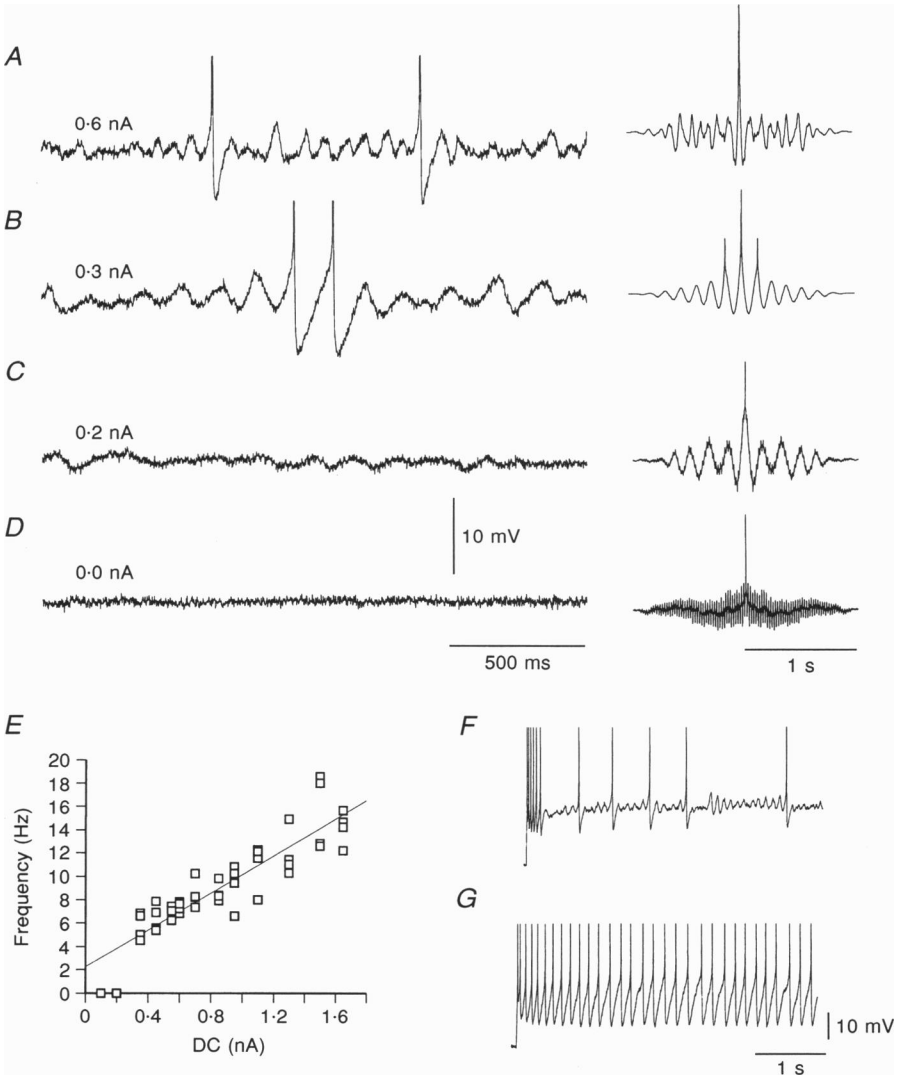


**Figure 2. The frequency of the subthreshold oscillations is voltage dependent**

*A–D*, membrane potential of the same neuron measured at different holding currents (indicated to left of traces). The right-hand traces show the corresponding autocorrelograms. At rest (*D*) the membrane voltage is stable. At +0·2 nA (*C*) small fluctuations in membrane voltage arise. With further depolarization (*A* and *B*) subthreshold oscillations become apparent with occasional action potential firing (the action potentials are truncated). *E*, plot of the subthreshold oscillation frequency as a function of the injected current. The slope of the linear regression is 7·9 Hz nA$^{-1}$, $r^2 = 0{\cdot}8$. *F* and *G*, different responses to prolong suprathreshold current pulse in two neurons. An oscillating response characterized by an initial burst followed by subthreshold oscillations and an occasional firing of an action potential (*F*). A non-oscillating response characterized by continuous firing with frequency adaptation (*G*). Note that the action potentials are truncated.

As mentioned above, not all cells demonstrated subthreshold oscillations. Compare the response of an oscillating (Fig. 2*F*) neuron to the response of a non-oscillating neuron (Fig. 2*G*). In the oscillating neuron intracellular injection of a current pulse (0·6 nA) elicited a brief burst of action potentials followed by a prolonged period of low amplitude oscillations which occasionally reached firing threshold. A similar current pulse injected into the non-oscillating cell generated continuous firing of action potentials. In the latter case, subthreshold oscillations were not detected at lower current inputs, and at higher values the firing rate of the cell increased.

In a few cells, changing the holding potential could change the behaviour of the cell, whereas other cells spontaneously switched from one mode of behaviour to another. Therefore we could not use this property to categorize cortical neurons. Because we did not detect any systematic correlation between the oscillatory nature of the neuron and the parameters shown in Table 1, we conjecture that the marked difference in the observed responses (compare Fig. 2*F* and *G*) may be due to small differences in membrane properties.

We exclude the possibility that the oscillations are aborted sodium spikes typical of fatigued neurons because oscillation amplitude was always smaller than 15 mV. Furthermore, unlike run-down phenomena, stable oscillatory activity was recorded for long periods.

### Ionic mechanism of the subthreshold oscillations

The ionic mechanism underlying the oscillations was examined by blocking membrane currents using TTX, TEA and $Co^{2+}$. The results are summarized in Fig. 3. DC injection, or prolonged current pulses, were used to elicit oscillations before and after addition of the blocker. The effect of TTX (approximately $10^{-6}$ M) is shown in Fig. 3*A*. The upper trace shows a control recording in which a train of action potentials was generated at the onset of the current injection, followed by sporadic periods of low amplitude oscillations with intermittent firing of single action potentials. The middle and lower traces show responses to the same current injections 1·5 and 2·5 min after the addition of TTX. Both the spikes and the subthreshold oscillations disappeared. A similar effect was observed in all cells tested with TTX ($n = 7$). The possibility that $Na^+$ current is involved in the generation of subthreshold oscillations was further strengthened by intracellular injection of QX-314 ($n = 5$). This latter experiment also demonstrated that the subthreshold oscillations are the property of individual cells and are not driven by synaptic input.

Figure 3*B* shows that the subthreshold oscillations are unaffected by $Co^{2+}$. Both traces depict the electrical activity of a neuron at a depolarized membrane potential before (upper trace) and 15 min after (lower trace) replacing the external solution with $Co^{2+}$ solution (see Methods). The depolarized level was due to DC injection and the magnitude of the current was adjusted so that both records were obtained at the same membrane potential. The presence of $Co^{2+}$ (5 mM) induced an increase in firing frequency, probably due to the blockade of a $Ca^{2+}$-dependent $K^+$ conductance, but essentially it did not effect the oscillations in membrane potential. Similar results were observed in two other cells.

The effect of TEA (15 mM) is illustrated in Fig. 3*C*. Under control conditions (upper trace), action potentials and low amplitude oscillations were recorded. Five minutes after replacing the external solution with TEA solution (lower trace), the electrical activity became dominated by rhythmic bursts of action potentials. Each burst consisted of two spikes and was followed by a prolonged after-hyperpolarization (AHP) that lasted for about 2 s. The voltage trajectory between bursts was devoid of oscillatory activity. The elimination of oscillatory activity may have been the result of the prolonged AHP and the accompanying changes in membrane conductance rather than the result of blocking $K^+$ conductance. To examine this possibility, the normal physiological solution was replaced in two experiments with a solution containing 15 mM TEA and 5 mM $Cs^+$, to block $K^+$ currents, and $Ni^{2+}$ (1 mM) to block $Ca^{2+}$ current and to eliminate the prolonged AHP. The absence of subthreshold oscillations under these conditions indicates that $K^+$ conductance is indeed involved in their generation.

We suggest that $Na^+$- and $K^+$-dependent conductances participate in the generation of subthreshold oscillations. This suggestion is in agreement with the conclusion of McCormick *et al.* (1985), that $Na^+$ and $K^+$ currents dominate the electrical activity of neocortical pyramidal cells at the subthreshold range of potentials.

### Impedance measurements

We explored the relationship between the subthreshold oscillations and the membrane properties in the frequency domain. Voltage responses of thirty neurons to intracellular injection of sinusoidal current with changing frequency (ZAP input) were analysed. In most cells a peak in the response (resonance) was observed (see arrows in Figs 1*A* and 4*A*). In cases where resonance behaviour could not be detected, the maximum response was recorded at low frequencies and, as expected for a passive RC circuit, the response decreased monotonically at higher frequencies (Fig. 4*B*).

To examine the effect of membrane potential on the response to ZAP stimuli, the membrane potential was shifted to different values by DC injections. Because at depolarized levels action potentials interfere with the analysis of the ZAP response, the first set of these experiments (shown in Figs 4 and 5) was conducted in the presence of TTX. Examples of the neuronal response to ZAP stimuli at two different membrane potentials are

shown in Fig. 4*A* and *B*. At resting potential (−66 mV, Fig. 4*B*) the maximum amplitude of the response appeared at the lowest frequencies (at the end of the stimuli). At the depolarized level (−50 mV, Fig. 4*A*) the maximum amplitude was reached about 2·5 s after the onset of the stimulus. Although the ZAP function in Fig. 4*A* and *B* had the same constant amplitude, the voltage response at resting level (Fig. 4*B*) displayed larger peak-to-peak amplitudes, particularly at low frequencies.

Figure 4*C* demonstrates smoothed impedance magnitude (IM) curves measured at different holding potentials for the same cell shown in Fig. 4*A* and *B*. As the holding

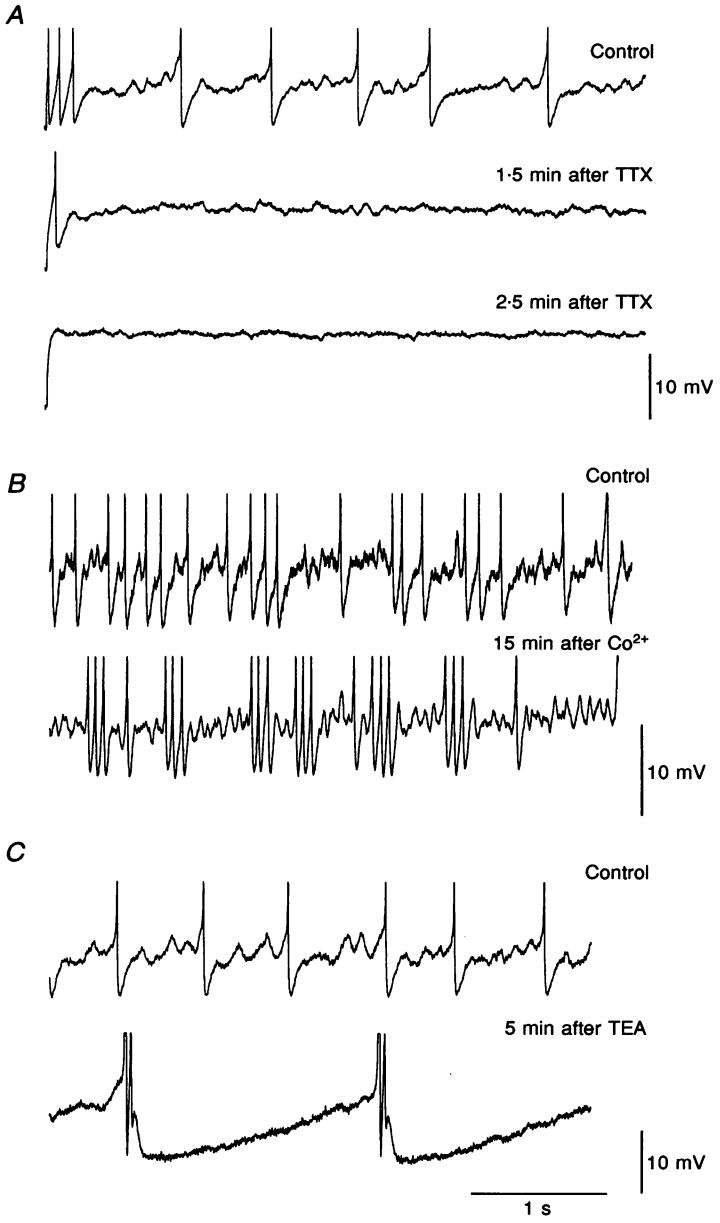


**Figure 3. Subthreshold oscillations are TTX and TEA sensitive but insensitive to $Co^{2+}$**

*A*, the effect of TTX. Control (upper trace) shows the voltage response following a long depolarizing current pulse. Subthreshold oscillations with intermittent action potentials were observed. Both spikes and subthreshold oscillations were abolished 2·5 min after application of 10 $\mu$M TTX. *B*, blocking $Ca^{2+}$ conductance does not abolish the subthreshold oscillations. The control is shown in the upper trace. Subthreshold oscillations were still apparent 15 min after exchanging the external solution with $Ca^{2+}$-free solution containing 5 mM $Co^{2+}$ (lower trace). *C*, the effect of TEA. The response in the lower trace was measured from the same cell and at the same holding potential as in the control (upper trace). Five minutes after exchanging the external solution with 15 mM TEA-containing solution the subthreshold oscillations were eliminated but not the action potentials. Note that the action potentials in *A*, *B* and *C* are truncated.

potential became depolarized the IM decreased and the peak frequency was shifted towards higher values. The plot at −66 mV (rest) peaked at a frequency of about 5 Hz (arrow in Fig. 4*C*). Depolarizing the membrane potential to −56, −53 and −50 mV shifted the resonance frequency to 6, 8 and 12 Hz, respectively. At low frequencies the IM decreased from 50 MΩ (measured at 2 Hz, −66 mV) to 15 MΩ (measured at 2 Hz, −50 mV). At high frequencies, however, the IM was independent of the holding potential and all curves converged.

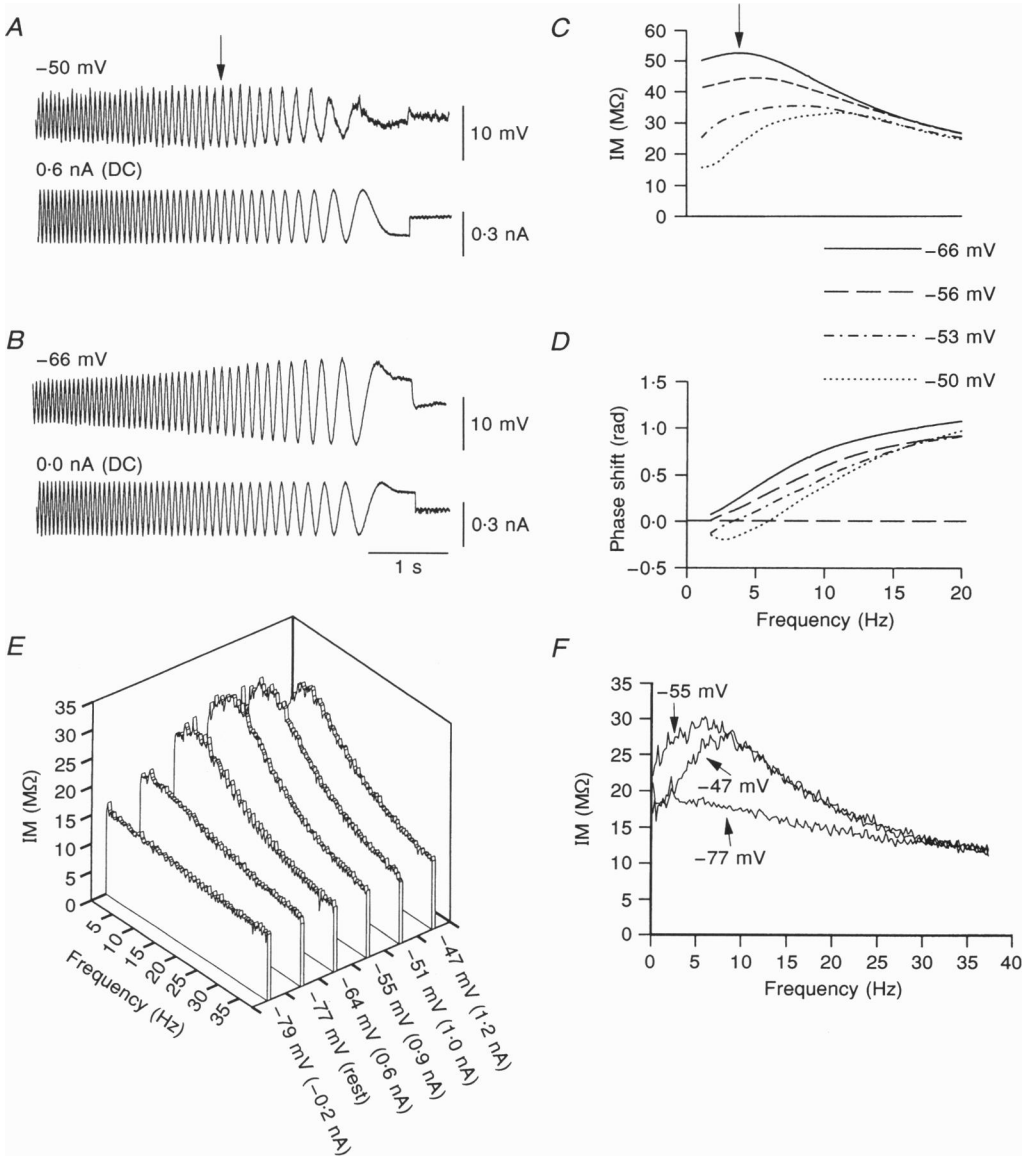


**Figure 4. The response to ZAP input is voltage dependent**

*A*, the voltage response of a TTX-treated cell (upper trace) to a ZAP input (lower trace) recorded at a membrane potential of −50 mV (+0·6 nA DC was injected to maintain the membrane potential). Maximal response was obtained 2·5 s after the stimulus onset (arrow). *B*, voltage response of the same cell as shown in *A* to a ZAP input measured at −66 mV (resting level). The maximal response occurred at the end of the stimulus (lowest frequencies). Note that, at low frequencies, the voltage response was larger than that observed at less negative membrane potential (Fig. 4*A*). *C*, smoothed IM plots calculated from the responses to ZAP inputs at different holding potentials, −66 to −50 mV. Depolarization decreased the amplitude of the IM plots and shifted the peak towards higher frequencies. *D*, smoothed phase shift plots obtained from the same data as shown in *C*. Depolarization introduced a negative phase shift at low frequencies. *E*, three-dimensional graph describing the IM plot (IM against frequency) at six different holding potentials measured in a different cell. Note that the IM plot at −55 mV has the highest values. *F*, three IM plots (taken from *E*) displayed on a two-dimensional graph. Note that the results shown in this figure were all measured in the presence of $10^{-6}$ M TTX.

Figure 4*D* shows smoothed phase shift curves. As the membrane potential was more depolarized, a negative phase (phase lag) appeared at low frequencies (Fig. 4*D*, −53 and −50 mV). Thus, the phase changed from negative to positive values, intersecting the zero line at a certain frequency (the zero phase frequency). The intersection point shifted to higher frequencies (to the right) as the membrane was further depolarized. At −53 mV the intersect was at 4 Hz, whereas at −50 mV it was between 6 and 7 Hz.

A reduction in the amplitude of the response to the ZAP input was apparent in both hyperpolarizing and depolarizing directions (Fig. 4*E* and *F*). Shifting the membrane potential from −64 to −77 and −79 mV resulted in successive decreases in IM values (Fig. 4*E*). Depolarization above −55 mV also resulted in a decrease in IM at low input frequencies (Fig. 4*F*). Thus, at a certain potential the IM (and the voltage response) was maximal.

The dependence of the IM peak frequency and the zero phase shift frequency on voltage is summarized for ten TTX-treated cells in Fig. 5. Both frequencies increased with depolarization and the zero phase shift frequency was always lower than the corresponding IM peak frequency. For each neuron the points were fitted by a straight line. A significant positive slope ($P < 0{\cdot}05$, linear regression Student's $t$ test) was found in eight of ten neurons. For the IM peak frequency, the mean slope was $0{\cdot}29 \pm 0{\cdot}11$ Hz mV$^{-1}$ (Fig. 5*A*), whereas for the zero phase shift frequency the slope was $0{\cdot}18 \pm 0{\cdot}08$ (Fig. 5*B*).

### Ionic mechanism of resonance behaviour

We examined the contribution of specific currents to the resonance behaviour. The effect of $10^{-6}$ M TTX application on the IM plots at two levels of membrane potential is shown in Fig. 6*A*. At resting level (left panel) the curves before (dashed line) and after (continuous line) the addition of TTX are basically similar. At a depolarized level, however, TTX caused a dramatic decrease in the impedance values in the whole range of 2–17 Hz (right panel). The two curves converge at 17 Hz, indicating that TTX-sensitive currents modulate the impedance only at frequencies lower than 17 Hz. This behaviour was observed in three of four cells examined.

The IM plot shown in Fig. 6*B* demonstrates the effect of adding 15 mM TEA and 5 mM $Cs^+$ to the external solution. The left panel shows the results obtained at resting potential, whereas the right panel shows the results measured at 10 mV above rest. Both experiments were conducted in the presence of TTX. The most prominent effect of blocking potassium conductance was the abolishment of the IM peak. TEA and $Cs^+$ increased the IM only at low frequencies; at high frequencies both curves converged. A much larger effect was observed at depolarized levels. At rest the IM changed from 70 to 90 MΩ at 1 Hz (Fig. 6*B*, left panel), whereas at 10 mV depolarization the corresponding change was from 40 to almost 100 MΩ (Fig. 6*B*, right panel). These results suggest that a voltage-dependent potassium conductance influences the impedance of these cells. The IM, measured 27 min after washing the slice with the control ringer (dotted line in right panel of Fig. 6*B*), demonstrated partial recovery of the effect. This experiment was repeated in three cells; all showed the same behaviour.

Two different solutions were used to eliminate $Ca^{2+}$ currents; one containing 5 mM $Co^{2+}$, the other 1 mM $Ni^{2+}$. In both cases external $Ca^{2+}$ concentration was reduced to zero. Figure 6*C* shows an example of the IM curves measured with $Ni^{2+}$ solution. The left panel shows the control curve (dashed line) and the curve obtained in the presence of $Ni^{2+}$ (continuous line). Both curves were obtained at a depolarized level of 15 mV and peaked at

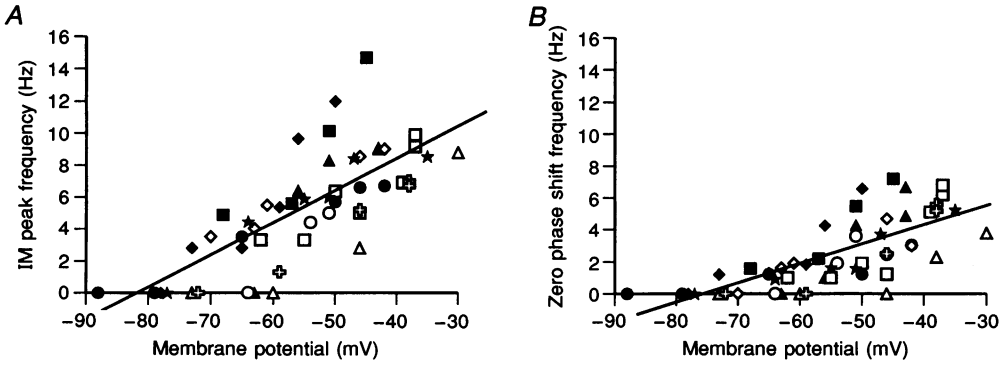


**Figure 5. The voltage dependence of the peak frequency and the zero phase shift frequency**

*A*, the IM peak frequency as a function of membrane potential measured in 10 cells (each represented by a different symbol), all treated with TTX. The linear regression slope is 0·2 Hz mV$^{-1}$ ($r^2 = 0{\cdot}52$). *B*, the zero phase shift frequency as a function of membrane potential measured from the same cells as shown in *A*. Note that, for any given voltage, the zero phase shift frequency is lower than the corresponding IM peak frequency. The linear regression slope is 0·12 Hz nA$^{-1}$ ($r^2 = 0{\cdot}5$).

7 Hz. There is no significant difference between the two curves. At a more depolarized level (23 mV above rest, Fig. 6*C*, right panel), the peak, in the solution containing $Ni^{2+}$, was reduced from 27 to 21 MΩ (22%). Both the control curve and the curve obtained in the presence of $Ni^{2+}$ peaked near 10 Hz. We examined the effect of $Ni^{2+}$ on four cells and the effect of $Co^{2+}$ on two cells. In all six cells the resonance behaviour (the peak in the IM plot) was not eliminated and the peak frequency was unaffected as a result of the treatment. The reduction in IM values around the peak shown in Fig. 6*C* was observed in four of the six cells examined. We conclude that at resting level the resonant behaviour is relatively insensitive to $Ca^{2+}$ currents blockers. However, at

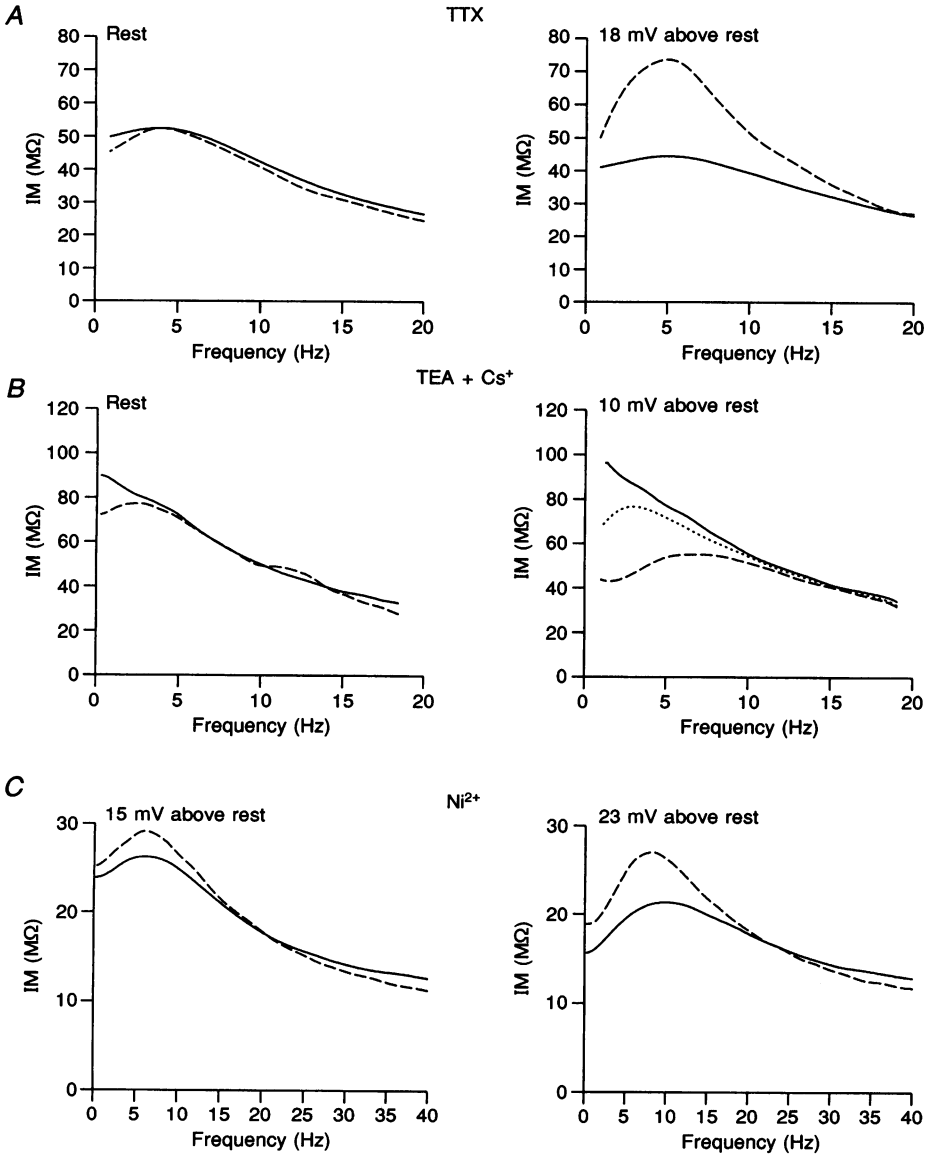


**Figure 6. The resonance behaviour is mostly TTX and TEA sensitive**

*A*, IM curves obtained before (dashed line) and after (continuous line) application of TTX (10 μM) at rest (left panel) and at a depolarized level (right panel). TTX made no change at rest, but 18 mV above rest it decreased the amplitude of the IM plot without changing the peak frequency. *B*, IM curves obtained before (dashed line) and after (continuous line) perfusing the slice with a solution containing 15 mM TEA and 5 mM $Cs^+$. The curves were calculated at rest (left panel) and at a depolarized level (right panel). TEA + $Cs^+$ caused an increase in IM values at low frequencies and eliminated the peak. Partial recovery was obtained after 27 min of perfusion with normal solution (dotted line in the right panel). *C*, IM curves obtained before (dashed line) and after (continuous line) substituting $Ni^{2+}$ for $Ca^{2+}$ in the external solution. The effect of $Ni^{2+}$ on the IM of a TTX-treated neuron is shown at two depolarized levels: 15 mV (left panel) and 23 mV (right panel) above rest. Note that a significant effect was observed only at strong depolarization.

strongly depolarized levels (> 20 mV) calcium currents activate and contribute to the impedance magnitude at the resonance frequency.

### The relationship between IM and the passive parameters ($R_{in}$ and $\tau_0$)

In order to determine the role of the passive properties of the neuron in shaping the IM plot, we calculated the expected relationship between the impedance and the input frequency in the case of an isopotential RC circuit. In such a case the impedance magnitude ($|Z|$) as a function of frequency ($f$) is:

$$|Z| = \frac{R_{in}}{\sqrt{(\tau_0^2 (2\pi f)^2 + 1)}}. \quad (7)$$

$R_{in}$ and $\tau_0$ were estimated by peeling the voltage responses to a short hyperpolarizing current pulse (see Methods). This procedure is expected to minimize the effect of the pulse itself on the various voltage-dependent conductances (Rapp *et al.* 1994). The experimental (continuous line) and the calculated (dashed line) IM plots shown in Fig. 7*A* were obtained in a TTX-treated cell. At low frequencies (up to 17 Hz) the measured values were smaller than the theoretical values and at higher frequencies both curves overlapped, indicating that, at these frequencies, the passive properties of the neuron can account for the shape of the IM plots.

Figure 7*B–E* shows additional comparisons between the theoretical passive and the experimental IM plots.

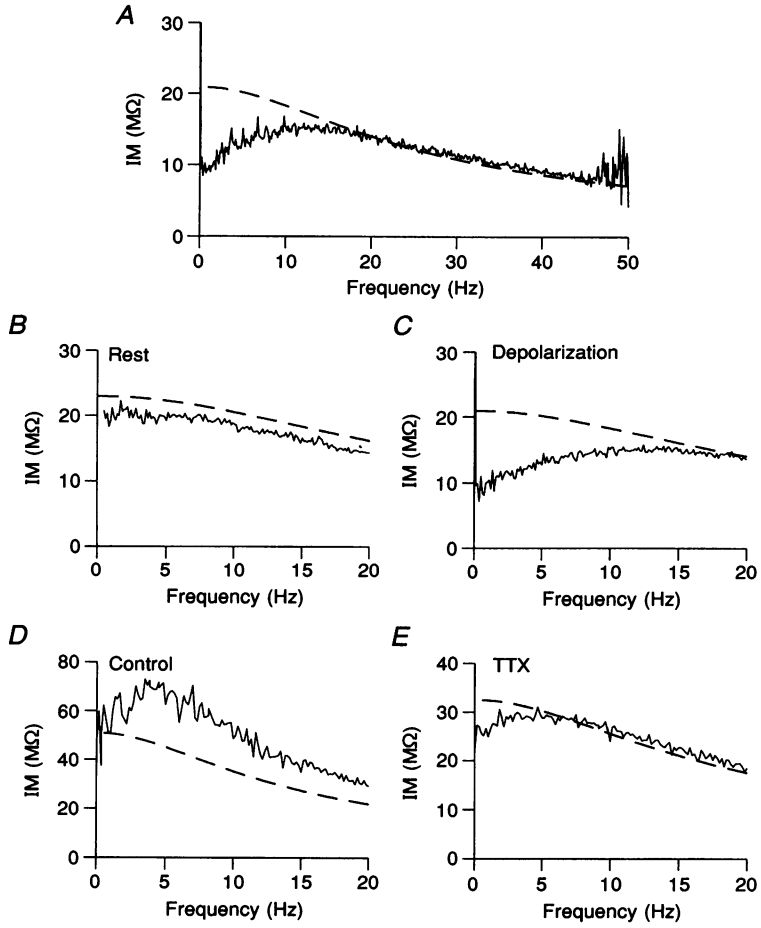


**Figure 7. Comparison between the measured IM plot and the theoretical passive plot**

IM curves (continuous line) were compared with theoretical passive IM curves (dashed line), calculated from the cell input resistance, $R_{in}$, and time constant $\tau_0$ (see Methods). $R_{in}$ and $\tau_0$ were measured from the voltage response to a short current pulse (0·6 ms, −3 nA). *A*, IM curves measured in the presence of TTX during +0·7 nA holding current. *B*, at resting level, the experimental IM agreed with the passive curve at all frequencies (up to 20 Hz). *C*, at depolarized level (17 mV above rest), the measured values were lower than the expected passive values (*B* and *C* were measured from the same cell). IM curves obtained before (*D*) and after (*E*) application of TTX (10 μM), both measured at a depolarized level of 10 mV above rest. Under normal conditions (*D*) the IM plot was above the expected passive values. After the addition of TTX, the IM curve matched the expected passive curve only at frequencies higher than 5 Hz.

Figure 7*B* shows results measured at rest (in the same cell as shown in *A*). In this case, although the expected values are about 3 MΩ larger than the measured values, the behaviour of both curves is similar. It seems that, at rest, the passive model fits the actual behaviour of the cell well. At the depolarized level (Fig. 7*C*) the measured impedance at zero frequency was about 10 MΩ while the expected impedance was 20·9 MΩ. The difference between the two curves decreased at higher frequencies. This difference can be accounted for by the presence of a slow current which is activated by depolarization, the reversal potential of which is more negative than the holding potential. Such a current will be more prominent at low frequencies and, when activated, it will tend to reduce voltage changes (and thus reduce the measured impedance). In principle the same effect may be obtained with a slowly inactivated current, the reversal potential of which is higher than the holding potential (Hatcheon *et al.* 1994). However, our conclusion that potassium current is involved (Fig. 6*B*) supports the first possibility.

Figure 7*D* and *E* compares the theoretical (dashed line) and the experimental (continuous line) IM plots, measured at 10 mV depolarization in normal conditions and after treating the cell with TTX. After adding TTX (Fig. 7*E*), the same behaviour described in Fig. 7*C* was obtained; at low frequencies the IM plot was below the predicted passive curve and above 5 Hz the experimental IM agreed with the passive IM. However, in normal conditions (Fig. 7*D*) the IM values are larger than the passive IM plot at all frequencies. This can be explained by the activation of a fast non-inactivating $Na^+$ current. Apparently, this current is capable of following the ZAP input even at high frequencies.

These results suggest that a fast TTX-sensitive current is responsible for the amplification of the IM (Figs 6*A* and 7*D*) and a slow current, which is activated with depolarization and has a reversal potential lower then the holding potential (probably $K^+$ current, see Fig. 6*B*), is responsible for damping voltage changes at low frequencies (Fig. 7*A* and *C*). The above conclusions form the basis for the model introduced in the following paragraph.

## Model results

The model is based on the current equations derived empirically by Yamada *et al.* (1989) to represent the slow $K^+$ current ($I_{K,s}$) and by French *et al.* (1990) to represent the fast persistent $Na^+$ current ($I_{Na,p}$). Utilizing the model we wish to examine qualitatively whether these two currents, plus the passive properties of the model neuron (assumed to be isopotential), are sufficient to produce sustained subthreshold oscillations and resonant behaviour as obtained experimentally.

The parameters for the $I_{K,s}$ were as for the IM current in Yamada *et al.* (1989). However, some of the parameters for the $I_{Na,p}$ current, described by French *et al.* (1990), were modified in order to obtain sustained voltage oscillations. A maximal conductance of 7·8 nS was measured by French *et al.* (1990) in the hippocampus; here we used 25 nS. The half-activation voltage of the corresponding conductance was shifted from the original −50 to −40 mV. The activation time constant for this current was not measured by French *et al.* (1990). For simplicity we used a constant $\tau_{Na,p}$ of 5 ms (see Discussion).

Qualitatively, the response of the modelled neuron to ZAP input is very much the same as that of a real neuron (Figs 8*A* and 9*C*). In both cases the response is highly

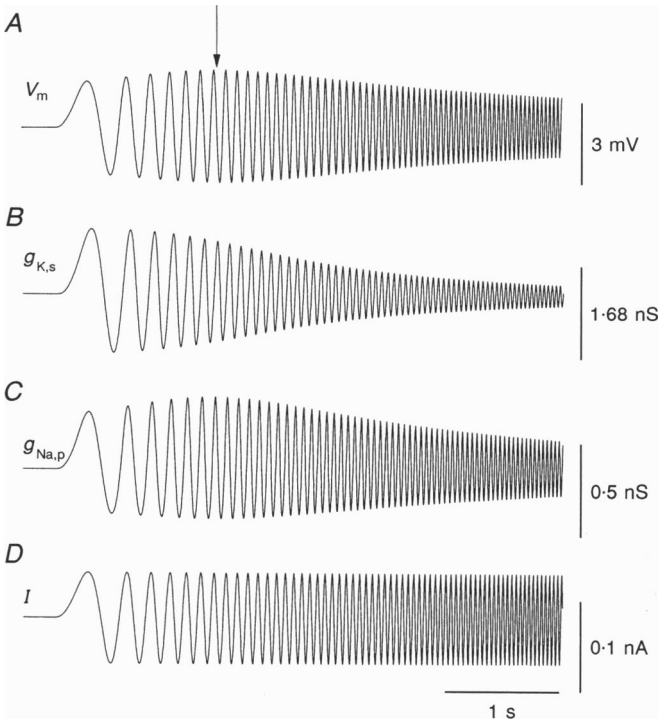


**Figure 8. The modelled voltage response and $Na^+$ and $K^+$ conductance during ZAP input**

The voltage response (*A*), the $K^+$ conductance (*B*) and the $Na^+$ conductance (*C*) were calculated during a response to a ZAP input (*D*). The amplitude of the changes in membrane potential reaches a peak value 1 s after the onset of the stimulus (arrow in *A*). The $K^+$ conductance changes (*B*) demonstrate a decline with frequency. The $Na^+$ conductance changes (*C*) resemble the changes in membrane voltage, reaching a peak value 1 s after the onset of the stimulus.

voltage dependent; IM changes from a monotonically declining function near rest (as in a passive case) to a resonant behaviour at the depolarized levels (Fig. 9*A*). In the model we dissect the relative contribution of each of the currents to the overall behaviour of the neuron. In Fig. 8 the changes in voltage ($V_m$, Fig. 8*A*), in $K^+$ conductance ($g_{K,s}$, Fig. 8*B*) and in $Na^+$ conductance ($g_{Na,p}$, Fig. 8*C*) during a ZAP input (Fig. 8*D*) are depicted. In this simulation, the holding potential was −59 mV (obtained with a DC of 0·2 nA). The maximal voltage change occurred at 7–8 Hz (arrow in Fig. 8*A*). Because $g_{K,s}$ has slow kinetics, it is most responsive at low frequencies at which it is capable of following the slow voltage changes (Fig. 8*B*). Thus, at low frequencies, $g_{K,s}$ was effective in damping the voltage changes. With increased frequency, $g_{K,s}$ was less effective and the voltage response to the ZAP input increased. At even higher frequencies, the capacitance of the model neuron dominated the voltage response and, as a result, the voltage response to the ZAP input decreased. This initial damping of the voltage response due to $g_{K,s}$ and the decline at high frequencies, due to the membrane capacitance, was reflected by a peak in the IM *vs.* frequency curve (Figs 9*A* and *D* and 10*B*). Unlike $g_{K,s}$, $g_{Na,p}$ followed the voltage at all frequencies and, therefore, it peaked at the same frequency as $V_m$ (Fig. 8*C*). Hence, $g_{Na,p}$ is responsible for the amplification of the response at frequencies near the peak.

Next we examined the model behaviour in the absence of the $Na^+$ current to simulate the experimental results under TTX conditions. Figure 9*A* and *B* demonstrates IM and phase shift plots calculated at different holding potentials. As the holding potential became depolarized, the IM decreased and the peak frequency shifted towards higher values. The theoretical phase shift curve (Fig. 9*B*) shows that as the membrane potential is more depolarized, a negative phase (phase lag) appears at low frequencies. The point of intersection with the zero line shifts to higher frequencies (to the right) as the membrane is further depolarized. Furthermore, the frequency at which intersection occurs is always lower than the frequency at which the corresponding IM curve peaks. These properties of the model agree with the experimental findings (Figs 4 and 5).

Figure 9*C* shows the voltage response with (upper trace) and without (lower trace) the $Na^+$ current. In both cases a peak frequency was observed. In the presence of a $Na^+$ current, the maximal peak-to-peak amplitude was larger. The corresponding IM plots in Fig. 9*D* show that removing the $Na^+$ current shifts the resonance frequency to higher values and reduces the impedance in the

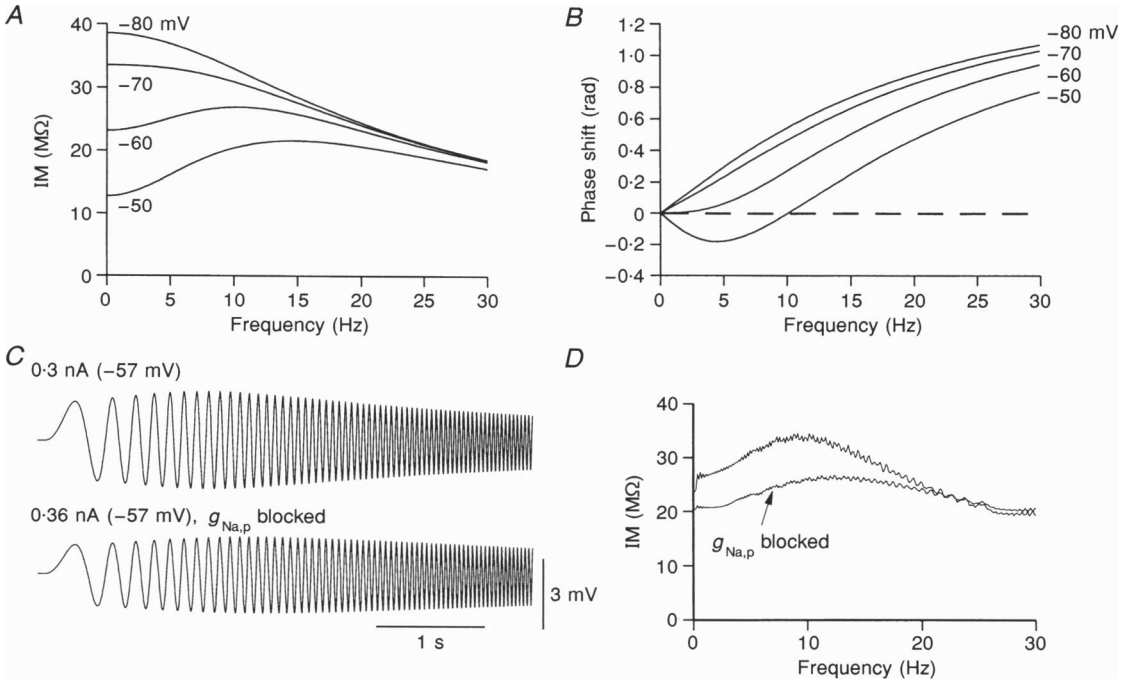


**Figure 9. The calculated IM and phase shift in a model without $Na^+$ conductance**

*A*, IM at different membrane potentials. Depolarization decreases the amplitude of the IM curves and shifts the peak towards higher frequencies. *B*, phase shift curves calculated in the same model as shown in *A*. Depolarization introduces a negative phase shift at low frequencies. *C*, the modelled response to a ZAP function at a membrane potential of −57 mV with (upper trace) and without (lower trace) $Na^+$ conductance. *D*, impedance magnitude curves calculated from the voltage responses shown in *C*. At frequencies lower than 20 Hz the absence of $Na^+$ current decreases the IM values and shifts the peak towards higher frequencies.

frequency range of 0–20 Hz. At higher frequencies, the IM values for both converge. The resonance behaviour of the model, with and without $Na^+$ current, agrees with the corresponding experimental results (i.e. with and without TTX, see Fig. 6*A*).

The model not only agrees with the resonance behaviour of cortical cells but also predicts oscillatory behaviour at a certain range of voltages. With a DC injection of 0·5 nA (Fig. 10*A*, lower trace) a steady voltage is developed. Increasing the DC level to 0·9 nA induces damped voltage oscillations at the beginning of the stimulus. A further increase (to 1·1 and 1·3 nA) results in sustained oscillations, whereas with a larger DC level (1·6 nA) the oscillations are essentially abolished (upper trace). The amplitude of the oscillations is voltage dependent yet, unlike the experimental results, the peak frequency remains constant at 7–8 Hz.

Next we examined the relationship between the peak IM frequency and the frequency of oscillations. The impedance of the model in a wide range of membrane potentials (Fig. 10*B*) was calculated analytically using the linear approximation method (see Methods and Appendix 2). The different voltage regimes in the time domain are marked on the voltage axis. The most clear feature of this graph is the pronounced and sharp peak (of about 300 MΩ) in the voltage range −45 to −40 mV. Sustained oscillations (7–8 Hz) were generated only in this limited range of voltages and damped oscillations appear on the steep slopes on both sides of this peak. Outside this range of voltage no oscillations were observed.

We also examined the behaviour of the model following the incorporation of the Hodgkin & Huxley (1952) spike mechanism. Two effects are apparent, an increase in the range of membrane potentials in which sustained subthreshold oscillations are attained (−49 to −35 mV)

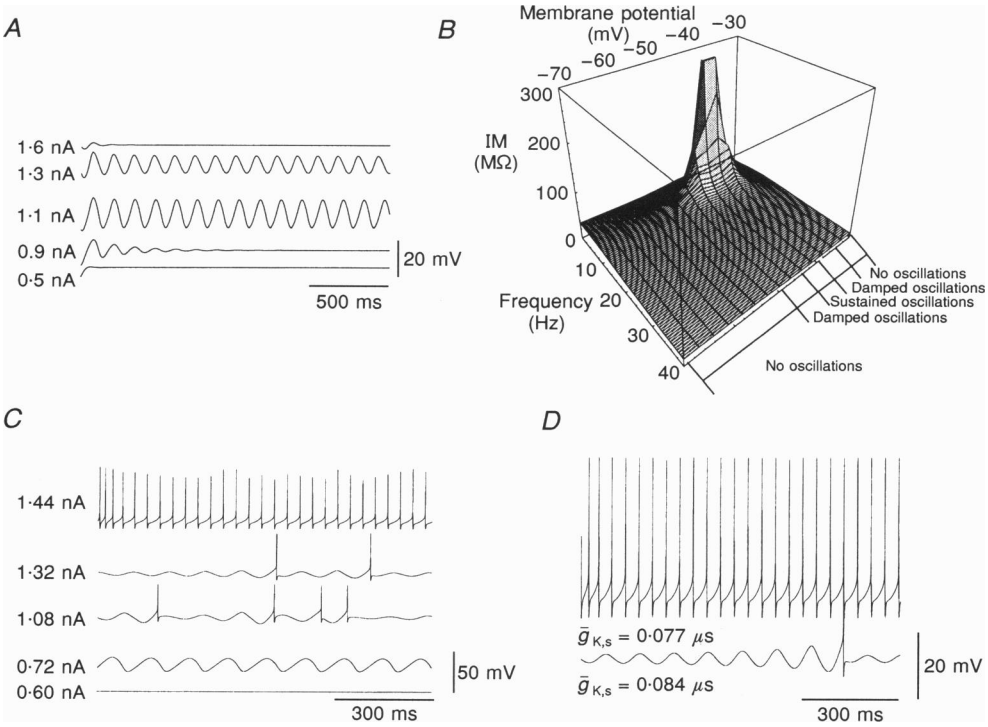


**Figure 10. The theoretical relationship between the subthreshold oscillations and the ZAP response**

*A*, membrane voltage calculated at different holding currents (from 0·5 to 1·6 nA). Damped oscillations are generated at 0·9 and 1·6 nA. Sustained oscillations are generated at 1·1 and 1·3 nA. *B*, the IM values as a function of frequency and voltage are shown in a three-dimensional graph. The different voltage behaviour regions (no oscillations, damped oscillations and sustained oscillations) are marked on the voltage axis. An immense peak in the IM plot was found at the same potentials where sustained oscillations were elicited. *C*, membrane potentials at different holding currents, calculated in a model that includes the Hodgkin & Huxley currents ($I_{K,d}$ and $I_{Na}$). The membrane potential shifts from steady-state to subthreshold oscillations then to subthreshold oscillations with intermittent spikes, finally reaching a state of continuous firing of action potentials. *D*, 10% decrease in the maximum value of the slow inactivating potassium conductance ($\bar{g}_{K,s}$) shifts the cell behaviour from a subthreshold oscillating potential (lower trace) to a continuously firing response.

and an increase in the variability of the amplitude (Fig. 10*C*). These two effects better describe the characteristics of the oscillations measured experimentally (see Fig. 2). A decrease in $\bar{g}_{K,s}$ (the maximum value of the slow potassium conductance) by only 10% is sufficient to produce a shift from a subthreshold oscillating potential (Fig. 10*D*, lower trace) to a continuously firing response (upper trace). In the following discussion we raise the possibility that the two different behavioural modes recorded in this study (Fig. 2*F* and *G*) reflect small changes in the slow potassium conductance.

## DISCUSSION

AC analysis is a powerful tool for exploring the electrical properties of nerve cells in the frequency domain (Puil *et al.* 1986; Correia *et al.* 1989). When combined with transient analysis, a more complete picture of the electrical behaviour of the neuron can be drawn. Indeed, in the present work we utilized both time- and frequency-domain analysis to understand the subthreshold electrical activity of cortical neurons. We conclude that the interplay between two currents, a slowly activating and non-inactivating $K^+$ current and a fast persistent $Na^+$ current can produce both subthreshold oscillations and resonance behaviour in cortical neurons. This conclusion was further investigated using a single-compartment neuron model. The model gave general insight into the ionic mechanisms of oscillations and elucidated the relationship between the oscillatory behaviour of cortical neurons and the response in the frequency domain. The main results and insights are summarized below.

### Mechanism of subthreshold oscillations

Subthreshold oscillations were found in 50% of the neurons in the frontal cortex. These subthreshold oscillations are clearly voltage dependent and are blocked by intracellular injection of QX-314. Therefore, they are generated by intrinsic cellular mechanisms rather than by a synaptic (network) mechanism. The subthreshold oscillations are both TTX and TEA sensitive, indicating the involvement of $Na^+$ and $K^+$ currents. Still, the ability of TTX to block the subthreshold oscillations does not prove that $Na^+$ currents participate directly in the generation of the oscillations. It is possible that sodium currents serve as an amplifier to increase small or distal oscillating currents. However, our modelling study suggests that a $Na^+$ current is indeed directly involved in the generation of these subthreshold oscillations.

From the ZAP response we deduced that the most dominant currents in the subthreshold response are a fast activating persistent $Na^+$ current and a slow non-inactivating $K^+$ current. The persistent $Na^+$ current ($I_{Na,p}$) will act to increase cell excitability, whereas the slow $K^+$ current ($I_{K,s}$) will tend to dampen excitability. Therefore, we propose that the difference between continuously firing cells (Fig. 2*G*) and oscillating cells (Fig. 2*F*) is in the relative magnitudes of $I_{K,s}$. A cell with a small $I_{K,s}$ (relative to $I_{Na,p}$) will tend to fire repetitively upon depolarization, whereas a cell with a larger $I_{K,s}$ will tend to generate subthreshold oscillations (see model results in Fig. 10*D*). Neuromodulators regulate some of these conductances (McCormick, Wang & Huguenard, 1993) and, therefore, in *in situ* conditions, could switch the cell from one mode of behaviour to another.

Sodium-dependent subthreshold oscillations with a similar range of frequencies ($8{\cdot}6 \pm 2{\cdot}1$) were reported also in the entorhinal cortex (Alonso & Klink, 1993; Klink & Alonso, 1993). Alonso & Klink (1993) suggested that an IM-like current is too slow to explain their experimental results and proposed that a fast activating $K^+$ current is involved in the generation of subthreshold oscillations, yet our modelling study demonstrates that a slow IM-like current is capable of producing oscillations.

### Functional significance of subthreshold oscillations

Although the subthreshold oscillations are, by definition, low amplitude phenomena, they may have important consequences for the input–output properties of the neuron (Laming, 1992; Alonso & Klink, 1993; Lampl & Yarom, 1993). For example, if excitatory inputs are coincident with the depolarizing phase of the subthreshold oscillations they are more likely to cause the cell to fire than if the same input coincides with the hyperpolarizing phase of the subthreshold oscillations (Lampl & Yarom, 1993). The duration of the oscillatory cycle, compared with the duration of the input, will determine the probability to reach threshold for firing (Laming, 1992). Also, in comparison to a steady depolarization, an oscillating depolarization will tend to inactivate inward currents to a lesser degree and, therefore, will increase the electroresponsiveness of the cell.

It has long been known that EEG recordings from the human brain reveal different rhythmic activities that are correlated with different behavioural states of sleep, arousal and awareness (Steriade *et al.* 1993). Is it possible that the subthreshold oscillations are the cellular basis for some of these rhythms (as speculated by Llinás *et al.* 1991)? Three lines of evidence support this possibility. First, the range of frequencies of the subthreshold oscillations overlap the range recorded with EEG techniques. Second, the subthreshold oscillation frequency is directly modulated by voltage; this mechanism may underlie the transition between different behavioural states. Accordingly, the different frequencies observed at different functional states (arousal, sleep and drowsiness) reflect different 'resting' levels, each of which corresponds to a different frequency of subthreshold oscillations in single cells. Changes in the resting level may be either due to changes in background activity (Bernander, Douglas, Martin & Koch, 1991; Rapp, Yarom & Segev, 1992) or the effect of neuromodulators (McCormick *et al.* 1993). Third, it is easy to reset the phase of the subthreshold oscillations

with a voltage perturbation. This property is essential for the synchronization of the subthreshold oscillations in the entire population, as required for the subthreshold oscillations to serve as the basis for EEG rhythms. Because subthreshold oscillations *per se* are not transmitted to neighbouring cells, such synchronization can only be achieved via spikes that ride on top of the subthreshold oscillations.

### Resonant behaviour

The oscillatory input (ZAP) was applied to explore the behaviour of the cortical neurons in the frequency domain. Utilizing this input, a resonant behaviour was revealed in the majority of the cells. The immediate implication of such resonance is that the neuron will respond more strongly to a specific input frequency. Thus, at the subthreshold level, the neurons are frequency selectors (bandpass filters). Significantly, at any given membrane potential, the preferred frequency of the neuron is in the same range as the subthreshold oscillation frequency. We speculate that the tendency of each neuron to generate voltage signals at a certain frequency and to preferentially respond to the same frequency will promote population activity at that preferred frequency.

There is a strong relationship between the subthreshold oscillations and the resonance behaviour. Both phenomena have the same basic frequencies and they depend on voltage in a similar way (Figs 2*E* and 5*A*). Their frequencies increase with depolarization and they are absent at strong hyperpolarizing potentials. Both phenomena are sensitive to $K^+$ blockers and are relatively insensitive to $Ca^{2+}$ blockers (Figs 3 and 6). We conclude that the same ionic mechanism that generates the subthreshold oscillations is also involved in the generation of the resonant behaviour. This conclusion was further supported by our modelling study (see below).

Two observations may seem to contradict this conclusion. First, both oscillating and non-oscillating neurons from the same population displayed resonant behaviour. Second, subthreshold oscillations are extremely sensitive to TTX (Fig. 3), whereas the impedance–frequency curve, although strongly affected, still showed resonant behaviour in the presence of TTX (Figs 6 and 7). To resolve this apparent conflict we conclude, on the basis of our modelling study, that resonant behaviour is an essential, yet insufficient, requirement for the generation of subthreshold oscillations (see below).

### The model

A biophysical membrane model was constructed based on the experimental observations which explored the minimal requirements for generating both subthreshold oscillations and resonance behaviour. The model was exploited both numerically, to simulate its voltage response, and analytically, to compute the impedance profile directly and to examine the contribution of the different model components to this profile. The analytical solution is based on a linear approximation. We found that the impedance magnitude obtained by the linear approximation and the numerical approach is practically identical for different voltages up to −50 mV, in which the region of sustained oscillations starts (not shown). This comparison was performed with a maximal ZAP response of 10 mV. The similarity between the numerical and the analytical results indicates the validity of the linear assumption for voltage perturbations smaller than 10 mV.

The model shows that the interplay between a leak current and two active currents (fast persistent $Na^+$ current and slow non-inactivating $K^+$ current) is sufficient to produce both resonance and voltage oscillations. The model predicts well the effect of TTX on both phenomena as found experimentally. A corresponding model to that presented here was recently published by Wang (1993). Other mechanisms for generating subthreshold oscillations and resonance behaviour, with corresponding modelling studies, were proposed recently by Hutcheon *et al.* (1994) to explain resonance behaviour in thalamic neurons.

Unlike the experimentally measured subthreshold oscillation, the oscillation frequency in the model is essentially voltage independent. One possible explanation is that the fixed (voltage-independent) time constant ($\tau_{Na,p} = 5$ ms) used in the model is responsible for this discrepancy. This possibility was examined using the model where $\tau_{Na,p}$ ranged from 1 to 6 ms both linearly with voltage or following the Hodgkin & Huxley (1952) kinetics for the $Na^+$ current scaled appropriately. Even with these changes the frequency of the subthreshold oscillations remained essentially voltage independent. A second possible explanation is that other currents and morphological complexities, not taken into consideration in this model, are involved in determining the voltage dependence of the subthreshold oscillations. Pyramidal cells are known to have a variety of different voltage- and ion-dependent currents (Lytton & Sejnowski, 1991) and it is very likely that these other currents contribute to the oscillation phenomena.

The model demonstrates that, although tightly linked, the resonance behaviour can appear without the presence of oscillations. The range of membrane voltages which demonstrates resonance in the IM plot is much wider than the range in which voltage oscillations can be generated. Sustained oscillations arise at a limited voltage range where a sharp peak in the IM plot exists (Fig. 10*B*). Outside this range of voltages only damped oscillations were generated. The resonance behaviour, compared with the sustained oscillations, is more robust and is observed at a wider range of potentials.

## APPENDIX 1

Figure 11 shows a schematic representation of the model. The neuron is represented by a single compartment consisting of a capacitor, a passive conductance ($g_{leak}$) and two time- and voltage-dependent conductances, one for $Na^+$ ($g_{Na,p}$) and one for $K^+$ ($g_{K,s}$). In some of the simulations we added Hodgkin–Huxley-like currents, a fast $Na^+$ current ($I_{Na}$) and a delayed $K^+$ rectifier ($I_{K,d}$).

The current equation of the model is given by eqn (3) above. The following section gives the expressions and parameter values for $I_{K,s}$, $I_{Na,p}$, $I_{K,d}$, $I_{Na}$ and $I_{leak}$.

$I_{K,s}$

$$I_{K,s} = \bar{g}_{K,s}\, n (V - E_K), \tag{A1.1}$$

where $\bar{g}_{K,s}$ is 0·084 μS, as in Yamada *et al.* (1989), $E_K$ is −80 mV and $n$ is the activation coefficient,

$$\frac{dn}{dt} = \frac{n_\infty - n}{\tau_{K,s}}, \tag{A1.2}$$

where

$$\tau_{K,s} = \frac{1000}{3{\cdot}3(e^{(V+35)/40} + e^{-(V+35)/20})} \frac{1}{3^{(T-22)/10}},$$

$$n_\infty = \frac{1}{1 + e^{-(V+35)/10}}, \tag{A1.3}$$

where $T$ is the temperature; in this work $T$ is 34 °C.

$I_{Na,p}$

$$I_{Na,p} = \bar{g}_{Na,p}\, m (V - E_{Na}),$$

$$\frac{dm}{dt} = \frac{m_\infty - m}{\tau_{Na,p}},$$

$$m_\infty = \frac{1}{1 + e^{-(V+40)/5}},$$

where $\bar{g}_{Na,p}$ is 0·022 μS, $E_{Na}$ is 40 mV and $\tau_{Na,p}$ is 5 ms.

$I_{K,d}$

$$I_{K,d} = \bar{g}_{K,d}\, n^4 (V - E_K).$$

The rate constants are:

$$\alpha_n = \frac{0{\cdot}01(-V-20)}{e^{(-V-20)/10} - 1} \quad \text{and} \quad \beta_n = 0{\cdot}125e^{(-V-30)/80},$$

$$\frac{dn}{dt} = 3^{(T-6{\cdot}3)/10}(\alpha_n(1 - n) - n\beta_n),$$

where $\bar{g}_{K,d}$ is 5 μS and $T$ is 34 °C.

$I_{Na}$

$$I_{Na} = \bar{g}_{Na}\, m_\infty^3\, h (V - E_{Na}).$$

The activation variable for the fast sodium current ($m$) is substituted by its steady-state variable ($m_\infty$). $\bar{g}_{Na}$ is 12·5 μS and $T$ is 34 °C.

$$\frac{dh}{dt} = 3^{(T-6{\cdot}3)/10}(\alpha_h(1 - h) - h\beta_h),$$

$$m_\infty = \frac{\alpha_m}{\alpha_m + \beta_m}.$$

The rate constants for $h$ are:

$$\alpha_h = 0{\cdot}07e^{(-V-30)/20} \quad \text{and} \quad \beta_h = \frac{1}{e^{-V/10} + 1}.$$

The rate constants for $m$ are:

$$\alpha_m = \frac{-(V+16)}{10(e^{(-V-16)/10} - 1)} \quad \text{and} \quad \beta_m = 4e^{(-V-41)/18}.$$

$I_{leak}$

$$I_{leak} = g_{leak}(V - E_{leak}),$$

where $g_{leak}$ is 0·025 μS and $E_{leak}$ is −65 mV.

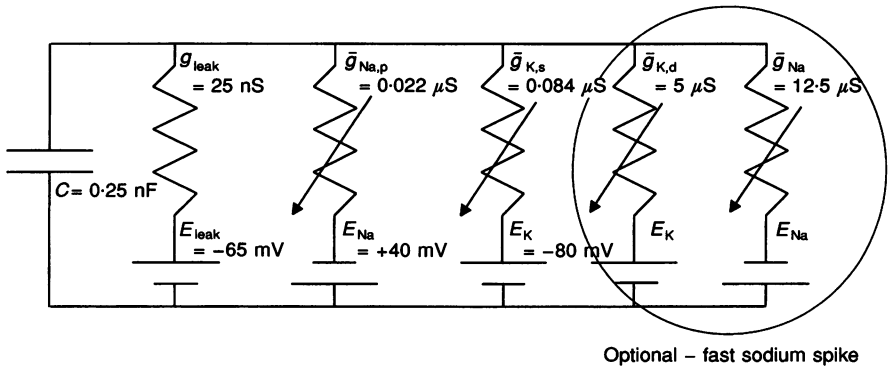


**Figure 11. Schematic representation of the model**

An isopotential membrane model composed of a capacitor and five parallel resistors. Four resistors represent the active conductances, $g_{Na,p}$, $g_{K,s}$, $g_{K,d}$ and $g_{Na}$ ($\bar{g}$ values given). The later two conductances represent the Hodgkin & Huxley (1952) mechanism for generating fast action potentials and were not used in all simulations. The constant resistor represents the passive (leak) conductance, $g_{leak}$. The ionic batteries for sodium, potassium and the leak current are marked by $E_{Na}$, $E_K$ and $E_{leak}$, respectively.

## APPENDIX 2

In this Appendix we derive the analytical expression for the model impedance. The total membrane current ($I$) is a sum of the capacitance current ($I_c$), the leak current ($I_{leak}$) and the active currents ($I_{K,s}$ and $I_{Na,p}$). We begin by calculating the impedance of the potassium current ($I_{K,s}$) given in eqn (A1.1). The differential of $I_{K,s}$ ($\delta I_{K,s}$) is:

$$\delta I_{K,s} = \bar{g}_{K,s} n_{SS} \delta V + \bar{g}_{K,s}(V_{SS} - E_K)\delta n. \quad \text{(A2.1)}$$

The subscript SS indicates that the variable is at the steady-state value. $\delta n$ is derived from eqn (A1.2), noting that the differential of $dn/dt$ is equal to the time derivative of $\delta n$,

$$\delta \frac{dn}{dt} = \frac{d(\delta n)}{dt} = \frac{\delta n_\infty}{\tau_{K,s}} - \frac{\delta n}{\tau_{K,s}} - \frac{(n_\infty - n_{SS})}{\tau_{K,s}^2}\delta\tau_{K,s}. \quad \text{(A2.2)}$$

$n_\infty$ is the steady-state value of $n$, hence $n_{SS} = n_\infty$ and eqn (A2.2) becomes:

$$\frac{d(\delta n)}{dt} = \frac{\delta n_\infty}{\tau_{K,s}} - \frac{\delta n}{\tau_{K,s}}. \quad \text{(A2.3)}$$

Because $n_\infty$ depends only on voltage, the differential of $n_\infty$ is:

$$\delta n_\infty = \left(\frac{dn_\infty}{dV}\right)\delta V. \quad \text{(A2.4)}$$

Substituting $\delta n_\infty$ in eqn (A2.4) with $\delta n_\infty$ from eqn (A2.3) we get

$$\frac{d(\delta n)}{dt} = \frac{1}{\tau_{K,s}}\frac{dn_\infty}{dV}\delta V - \frac{\delta n}{\tau_{K,s}}. \quad \text{(A2.5)}$$

Rearranging eqn (A2.5),

$$\left(\frac{d}{dt} + \frac{1}{\tau_{K,s}}\right)\delta n = \left(\frac{1}{\tau_{K,s}}\frac{dn_\infty}{dV}\right)\delta V. \quad \text{(A2.6)}$$

Introducing $\delta n$ in eqn (A2.6) to eqn (A2.1) gives,

$$\delta I_{K,s} = \left(\bar{g}_{K,s} n_{SS} + \frac{\bar{g}_{K,s}(V_{SS}-E_K)\left(\frac{1}{\tau_{K,s}}\frac{dn_\infty}{dV}\right)}{p + \frac{1}{\tau_{K,s}}}\right), \quad \text{(A2.7)}$$

where $p \equiv \frac{d}{dt}$.

It is evident from eqn (A2.7) that the reactance $\delta I_{K,s}/\delta V$ is composed of two components,

$$g_1 = \bar{g}_{K,s} n_{SS}, \quad \text{(A2.8)}$$

and

$$g_2 = \frac{\bar{g}_{K,s}(V_{SS}-E_K)\left(\frac{1}{\tau_{K,s}}\frac{dn_\infty}{dV}\right)}{p + \frac{1}{\tau_{K,s}}}, \quad \text{(A2.9)}$$

the derivative of $n_\infty$ with respect to $V$ is directly obtained from eqn (A1.3).

For simplicity we define,

$$a_{K,s} = \bar{g}_{K,s}(V_{SS} - E_K)\left(\frac{1}{\tau_{K,s}}\frac{dn_\infty}{dV}\right), \quad \text{(A2.10)}$$

and

$$b_{K,s} = \frac{1}{\tau_{K,s}}. \quad \text{(A2.11)}$$

The reciprocal values of $g_1$ and $g_2$ are the corresponding impedances, $Z_1$ and $Z_2$ composing the impedance, $Z_{K,s}$, of the $I_{K,s}$ current,

$$Z_{K,s1} = \frac{1}{\bar{g}_{K,s} n_{SS}}; \; Z_{K,s2} = \frac{1}{a_{K,s}}p + \frac{b_{K,s}}{a_{K,s}}.$$

Thus, $Z_{K,s}$ can be described by a circuit composed of two branches in parallel, $Z_{K,s1}$ is a pure resistor, whereas $Z_{K,s2}$ is an inductor ($L = 1/a_{K,s}$) in series with a resistor ($R = b_{K,s}/a_{K,s}$).

The impedance for the $Na^+$ current is calculated in exactly the same manner,

$$Z_{Na,P1} = \frac{1}{\bar{g}_{Na,p} m_{ss}} \text{ and } Z_{Na,p2} = \frac{1}{a_{Na,p}}p + \frac{b_{Na,p}}{a_{Na,p}}.$$

The impedance of the capacitor and the leak current are:

$$Z_C = 1/C_p \text{ and } Z_{leak} = 1/g_{leak}, \text{ respectively.}$$

The overall impedance, $Z$, is then,

$$Z = \left(\frac{1}{Z_{K,s1}} + \frac{1}{Z_{K,s2}} + \frac{1}{Z_{Na,p1}} + \frac{1}{Z_{Na,p2}} + \frac{1}{Z_C} + \frac{1}{Z_{leak}}\right)^{-1}. \quad \text{(A2.12)}$$

ADRIAN, E. D. & MATTHEWS, B. H. C. (1934). The Berger rhythm: potential changes from the occipital lobes in man. *Brain* **57**, 355–385.

ALONSO, A. & KLINK, R. (1993). Differential electroresponsiveness of stellate and pyramidal-like cells of medial entorhinal cortex layer II. *Journal of Neurophysiology* **70**, 144–157.

BERNANDER, O., DOUGLAS, R .J., MARTIN, K. A. C. & KOCH, K. (1991). Synaptic background activity influences spatiotemporal integration in single pyramidal cells. *Proceedings of the National Academy of Sciences of the USA* **88**, 11569–11573.

BRACEWELL, R. B. (1986). *The Fourier Transform and its Applications*, 2nd edn. McGraw-Hill International Editions.

CONNORS, B. W., GUTNICK, M. J. & PRINCE, D. A. (1982). Electrophysiological properties of neocortical neurons *in vitro*. *Journal of Neurophysiology* **48**, 1302–1320.

CORREIA, M. J., CHRISTENSEN, B. N., MOORE, L. E. & LANG, D. G. (1989). Studies of solitary semicircular canal hair cells in the adult pigeon. I. Frequency and time domain analysis of active and passive membrane properties. *Journal of Neurophysiology* **62**, 924–934.

CRAWFORD, A. C. & FETTIPLACE, R. (1981). An electrical tuning mechanism in turtle cochlear hair cells. *Journal of Physiology* **312**, 377–412.

DURAND, D., CARLEN, P. L., GUREVICH, N., HO, A. & KUNOV, H. (1983). Electronic parameters of neurons following chronical ethanol consumption. *Biophysical Journal* **54**, 807–817.

ERMENTROUT, B. (1990). *Phaseplane, Version 3.0, the Dynamical Systems Tool*. Brooks–Cole Publishing Company, CA, USA.

FRENCH, C. R., SAH, P., BUCKETT, K. J. & GAGE, P. W. (1990). A voltage-dependent persistent sodium current in mammalian hippocampal neurons. *Journal of General Physiology* **95**, 1139–1157.

GETING, P. A. (1989). Reconstruction of small neural networks. In *Methods in Neuronal Modeling*, ed. SEGEV, I. & KOCH, C., pp. 171–194. MIT Press, MA, USA.

GIMBARZEVSKY, B., MIURA, R. M. & PUIL, E. (1984). Impedance profiles of peripheral and central neurons. *Canadian Journal of Physiology and Pharmacology* **62**, 460–462.

GRAY, C. M., KONIG, P., ENGEL, A. K. & SINGER, W. (1989). Oscillatory responses in cat visual cortex exhibit inter-columnar synchronization which reflects global stimulus properties. *Nature* **338**, 334.

GUTFREUND, Y., YAROM, Y. & SEGEV, I. (1992). Resonant frequencies in guinea-pig cortical neurons and their relationship to subthreshold oscillations. *European Neuroscience Association* **3081**.

HODGKIN, A. L. & HUXLEY, A. F. (1952). A quantitive description of membrane current and its application to conduction and excitation in nerve. *Journal of Physiology* **117**, 500–544.

HUTCHEON, B., MIURA, R., YAROM, Y. & PUIL, E. (1994). Low threshold calcium current and resonance in thalamic neurons: a model of frequency preference. *Journal of Neurophysiology* **71**, 583–594.

KLINK, R. & ALONSO, A. (1993). Ionic mechanisms for the subthreshold oscillations and differential electroresponsiveness of medial entorhinal cortex layer II neurons. *Journal of Neurophysiology* **70**, 144–157.

KOCH, C. (1984). Cable theory in neurons with active linearized membrane. *Biological Cybernetics* **50**, 15–33.

LAMING, P. R. (1992). Information processing and neuromodulation in the visual system of frogs and toads. *Network* **3**, 71–88.

LAMPL, I. & YAROM, Y. (1993). Subthreshold oscillations of the membrane potential: a functional synchronizing and timing device. *Journal of Neurophysiology* **70**, 2181–2186.

LLINÁS, R., GRACE, A. A. & YAROM, Y. (1991). *In vitro* neurons in mammalian cortical layer 4 exhibit intrinsic oscillatory activity in the 10 to 50 Hz frequency range. *Proceedings of the National Academy of Sciences of the USA* **88**, 897–901.

LLINÁS, R. & YAROM, Y. (1986). Oscillatory properties of guinea-pig inferior olivary neurones and their pharmacological modulation: an *in vitro* study. *Journal of Physiology* **376**, 163–182.

LUPARELLO, T. J. (1967). *Stereotaxic Atlas of the Forebrain of the Guinea-pig*. Williams and Wilkins, Baltimore, MD, USA.

LYTTON, W. W. & SEJNOWSKY, T. S. (1991). Simulations of cortical pyramidal neurons synchronized by inhibitory interneurons. *Journal of Neurophysiology* **66**, 1059–1079.

MCCORMICK, D. A., CONNORS, B. W., LIGHTHALL, J. W. & PRINCE, D. A. (1985). Comparative electrophysiology of pyramidal and sparsely spiny stellate neurons of the neocortex. *Journal of Neurophysiology* **54**, 782–806.

MCCORMICK, D. A., WANG, Z. & HUGUENARD, J. (1993). Neurotransmitter control of neocortical neuronal activity and excitability. *Cerebral Cortex* **3**, 387–398.

MAURO, A., CONTI, F., DODGE, F. & SCHOR, R. (1970). Subthreshold behavior and phenomenological impedance of the squid giant axon. *Journal of General Physiology* **55**, 497–523.

MEYER, J. H. & ZAKON, H. H. (1982). Androgens alter the tuning of electroreceptors. *Science* **217**, 635–637.

PUIL, E., GIMBARZEVSKY, B. & MIURA, R. M. (1986). Quantification of membrane properties of trigeminal root ganglion neurons in guinea-pig. *Journal of Neurophysiology* **55**, 995–1016.

PUIL, E., MEIRI, H. & YAROM, Y. (1994). Resonant behavior and frequency preferences of thalamic neurons. *Journal of Neurophysiology* **71**, 575–582.

RAPP, M., SEGEV, I. & YAROM, Y. (1994). Physiology, morphology and detailed passive models of cerebellar Purkinje cells. *Journal of Physiology* **474**, 101–118.

RAPP, M., YAROM, Y. & SEGEV, I. (1992). The impact of parallel fibre background activity on the cable properties of cerebellar purkinje cells. *Neural Computation* **4**, 518–533.

RALL, W. (1969). Time constants and electronics length of membrane cylinders in neurons. *Biophysical Journal* **9**, 1483–1508.

SILVA, L. R., AMITAI, Y. & CONNORS, B. W. (1991). Intrinsic oscillations of neocortex generated by layer 5 pyramidal neurons. *Science* **251**, 432–435.

STERIADE, M., JONES, E. G. & LLINÁS, R. R. (1990). *Thalamic Oscillations and Signalling*. John Wiley & Sons, New York.

STERIADE, M., MCCORMICK, D. A. & SEJNOWSKI, T. J. (1993). Thalamocortical oscillations in the sleeping and aroused brain. *Science* **262**, 679–685.

WANG, X. J. (1993). Ionic basis for intrinsic 40 Hz neuronal oscillations. *NeuroReport* **5**, 221–224.

WILLCOX, K. S., GUTNICK, M. J. & CHRISTOPH, G. R. (1988). Electrophysiological properties of neurons in the lateral habenula: *in vitro* study. *Journal of Neurophysiology* **59**, 212–225.

YAMADA, W. M., KOCH, C. & ADAMS, P. R. (1989). Multiple channels and calcium dynamics. In *Methods in Neuronal Modeling*, ed. SEGEV, I. & KOCH, C., pp. 97–133. MIT Press, MA, USA.

**Acknowledgements**

We would like to thank Dr Bill Ross for his critical comments on this manuscript and to Dr Ilan Lampl for his help throughout the work. This work was supported by grants from the ONR, the Israeli Academy of Science and the Israeli Ministry of Science and the Arts.

*Received 11 March 1994; accepted 25 August 1994.*